MOLECULAR MACHINES

# A precise polyrotaxane synthesizer

Yunyan Qiu[1], Bo Song[1,2], Cristian Pezzato[1]*, Dengke Shen[1], Wenqi Liu[1], Long Zhang[1], Yuanning Feng[1], Qing-Hui Guo[1], Kang Cai[1], Weixingyue Li[1], Hongliang Chen[1], Minh T. Nguyen[1], Yi Shi[1], Chuyang Cheng[1]†, R. Dean Astumian[3]‡, Xiaopeng Li[2]‡, J. Fraser Stoddart[1,4,5]‡

Mechanically interlocked molecules are likely candidates for the design and synthesis of artificial molecular machines. Although polyrotaxanes have already found niche applications in exotic materials with specialized mechanical properties, efficient synthetic protocols to produce them with precise numbers of rings encircling their polymer dumbbells are still lacking. We report the assembly line–like emergence of poly[*n*]rotaxanes with increasingly higher energies by harnessing artificial molecular pumps to deliver rings in pairs by cyclical redox-driven processes. This programmable strategy leads to the precise incorporation of two, four, six, eight, and 10 rings carrying 8+, 16+, 24+, 32+, and 40+ charges, respectively, onto hexacationic polymer dumbbells. This strategy depends precisely on the number of redox cycles applied chemically or electrochemically, in both stepwise and one-pot manners.

The burgeoning of research on mechanically interlocked molecules (MIMs) (*1*) has contributed to progress in the design and synthesis of artificial molecular machines (AMMs) (*2*, *3*). The growing impact of the mechanical bond (*4*) on polymer chemistry and materials science, on the other hand, has led to the development of macroscopic soft materials with unusual properties (*5*). Among these materials, mechanically interlocked polymers (MIPs), such as polyrotaxanes (*6*, *7*) and polycatenanes (*8*, *9*), with complex architectures and topologies, respectively, are desirable synthetic targets that permit access to applications in areas such as slide-ring gels (*10*), battery electrode materials (*11*), and drug delivery platforms (*12*, *13*). These MIPs are usually prepared by template-directed protocols (*14*) that rely on molecular recognition (*15*) and self-assembly (*16*), depending on the synergy between supramolecular chemistry and polymer science.

One of the simplest and most general synthetic strategies for preparing polyrotaxanes is the so-called "threading followed by stoppering" approach (*17*), which takes advantage of noncovalent bonding interactions between polymeric axles and threaded rings with a range of threading kinetics (*18*) to form pseudopolyrotaxanes (*19*), after which bulky stoppers can be connected covalently to both ends of the polymer chains to prevent the loss of the rings by slippage (*20*). The synthesis of polyrotaxanes involving poly(ethylene glycol) (PEG) and cyclodextrins (*17*), exploiting the hydrophobic effect in water, is perhaps the most representative case using this strategy, affording slide-ring materials with remarkable physical properties (*10*) attributable to their mobile ring components. However, certain limitations intrinsically associated with the nature of this synthetic approach appear to be evident, such as (i) restricted control over the number and density of the threaded rings and (ii) limited access to other types of polymer axles displaying weaker or no appreciable noncovalent bonding interactions with the rings.

Oligo- and polyrotaxanes with partial or restricted control over the numbers and densities of the rings have been obtained by several approaches, such as template-directed clipping reactions (*21*, *22*), dynamic acyclic diene metathesis polymerization (*23*), ring-opening olefin metathesis polymerization (*24*), covalent synthesis (*25*), and iterative active-template synthesis (*26*). These strategies can regulate, to differing extents, the numbers, densities, and/or positions of the rings encircling oligo- and polymer axles, leading to enhanced control and distribution of the mobile rings, which serve as a crucial factor in determining and tuning the physical properties of these polyrotaxanes (*27*). Nonetheless, synthetic methodologies, involving precise control over the numbers of rings threaded onto polymers that interact weakly with the rings, are few and far between. We envisioned that a precisely controlled synthetic protocol, harnessing AMMs in delivering rings sequentially onto polymer chains, could give rise to MIPs with flawless control over the numbers of mechanical bonds, the formation of which can be independent of the nature of the chosen polymer dumbbells as a result of the high operational reliability of AMMs. Our synthetic strategy receives its inspiration from the redox-driven artificial molecular pump (AMP), which has been used (*28*–*30*) to recruit cyclobis(paraquat-*p*-phenylene) (**CBPQT$^{4+}$**) rings from bulk solution onto relatively short oligomeric collecting chains, thus resulting in the production of MIMs away from equilibrium.

Here, we report the precision synthesis (Fig. 1) of enthalpically and entropically demanding multicationic poly[*n*]rotaxanes, in which PEG serves as the centrally located collecting chain in the polymer dumbbells and CBPQT$^{4+}$ as the threaded rings; PEG has been chosen and recognized (figs. S82 to S87) to display no appreciable noncovalent bonding interactions with these rings in acetonitrile. Complete control over the number (up to 10) of rings mechanically interlocked with an individual polymer chain has been realized through the incorporation (Fig. 1A) of two redox-operated AMPs, which are covalently attached to both ends of PEG. These polymer dumbbells can therefore confer on the collecting chains the flawless ability to accommodate multiple ring components sequentially. The pumping of these rings onto the polymer dumbbells is powered precisely by the redox-switching properties of the bipyridinium units associated with both the rings and the AMPs, using an energy-ratchet mechanism (*2*, *31*) reported previously (*28*–*30*). In this manner, two **CBPQT$^{4+}$** rings can be pumped simultaneously onto the collecting polymer chains after each redox cycle. A defined number of rings (2, 4, 6, 8, and 10) can then be installed (Fig. 1B) onto the collecting PEG chains, depending solely on the number of redox cycles applied to both the AMP-functionalized polymer dumbbells and the **CBPQT$^{4+}$** rings.

The polymer dumbbell **PolyDB$^{6+}$** (Fig. 2A) incorporating two AMPs at both ends of the azide-terminated PEG (number-average molecular weight $M_n$ = 2000, polydispersity $Đ$ = 1.05) (*32*) was synthesized (fig. S1) using click chemistry (*33*) and has been characterized (fig. S3) by $^1$H nuclear magnetic resonance (NMR) spectroscopy. The AMP (Fig. 2A) consists of a bipyridinium (BIPY$^{2+}$) unit positioned between a 2,6-dimethylpyridinium (PY$^+$) coulombic barrier and an isopropylphenylene (IPP) steric barrier, which, taken as a trio, gives access to the formation of mechanical bonds with the CBPQT$^{4+}$ rings. The operation of the two-terminal AMPs relies on the redox-switching properties of BIPY$^{2+}$ units associated with both the molecular pumps and the rings. Upon reduction, all BIPY$^{2+}$ units are reduced to their radical cationic states, leading to the threading of two **CBPQT$^{2(•+)}$** rings onto **PolyDB$^{4(+)2(•)}$** (Fig. 2B, II), with the formation of two trisradical tricationic complexes based on radical-radical interactions (*34*). After oxidation, the strong coulombic repulsions between charged units force the rings to traverse the IPP units (Fig. 2B, III) by exploiting the imbalance between the energy barriers exerted from the charged (PY$^+$ and BIPY$^{2+}$) units of the pumps and the neutral IPP units, resulting in the formation of the poly[3]rotaxane

[1]Department of Chemistry, Northwestern University, Evanston, IL 60208, USA. [2]Department of Chemistry, University of South Florida, Tampa, FL 33620, USA. [3]Department of Physics, University of Maine, Orono, ME 04469, USA. [4]Institute for Molecular Design and Synthesis, Tianjin University, Tianjin 300072, P. R. China. [5]School of Chemistry, University of New South Wales, Sydney, NSW 2052, Australia.
*Present address: Institut des Sciences et Ingénierie Chimiques, Ecole Polytechnique Fédérale de Lausanne (EPFL), 1015 Lausanne, Switzerland.
†Present address: College of Chemistry, Sichuan University, Chengdu, Sichuan 610064, P. R. China.
‡Corresponding author. Email: astumian@maine.edu (R.D.A.); xiaopengli1@usf.edu (X.L.); stoddart@northwestern.edu (J.F.S.)

during thermal relaxation (Fig. 2B, IV). A second redox cycle following an analogous mechanism produces the poly[5]rotaxane (Fig. 2B, V, VI, and VII), and so on.

The polyrotaxane synthesizer is operated by an energy-ratchet mechanism (*2*, *31*). The fundamental operation principle relies on the fact that the energy of the electrostatic barriers arising from the $PY^+$ and $BIPY^{2+}$ units and of the radical-pairing interactions forming tris-radical tricationic complexes depends strongly on the redox state of the system, whereas the heights of the steric barriers imposed by the IPP units are independent of the redox state (Fig. 2B). The resulting kinetic asymmetry (fig. S2) allows the pumps to use the energy supplied by the alternating redox reagents or potentials to drive the formation of a highly nonequilibrium mechanically interlocked system—a polyrotaxane with up to 10 rings threaded onto a collecting chain—that persists as a metastable state away from equilibrium for a long time.

First, we subjected **PolyDB**$^{6+}$ and a large excess of **CBPQT**$^{4+}$ to one cycle of redox reactions using cobaltocene (reductant) and $NOPF_6$ (oxidant) (*35*). Subsequent $^1$H NMR spectroscopic analysis (fig. S4) confirmed the successful production of the poly[3]rotaxane **S-PR2**$^{14+}$ (**S** denotes stepwise) with only two mechanically interlocked $CBPQT^{4+}$ rings, showing that both AMPs operate simultaneously. Motivated by this accomplishment, we decided to apply a stepwise synthetic strategy to the isolated poly[3]rotaxane **S-PR2**$^{14+}$ that was used as the starting material, and subsequently generated the poly[5]rotaxane **S-PR4**$^{22+}$ with four $CBPQT^{4+}$ rings after a second redox cycle. A repeat of this redox cycle led to the poly[7]rotaxane **S-PR6**$^{30+}$ with six mechanically interlocked rings, using **S-PR4**$^{22+}$ as the starting material. All three poly[*n*]rotaxanes have been characterized (figs. S4 to S6) by $^1$H NMR spectroscopy.

The ease of the redox operation of the AMPs simply by the addition of redox reagents, as well as a relatively short operating time (within 1 hour) for each redox cycle, also led us to the adoption of a one-pot synthetic strategy, which eliminates the tedious isolation of intermediate poly[*n*]rotaxane precursors. Accordingly, **O-PR2**$^{14+}$, **O-PR4**$^{22+}$, and **O-PR6**$^{30+}$ (**O** denotes one-pot) can be produced by subjecting **PolyDB**$^{6+}$ to one, two, and three redox cycles, respectively, through the repetitive, alternating addition of reductant and oxidant into the reaction mixture. We then continued the redox cycle, producing the poly[9]rotaxane **O-PR8**$^{38+}$ and the poly[11]rotaxane **O-PR10**$^{46+}$ with corresponding numbers of 8 and 10 rings, respectively. All these poly[*n*]rotaxanes produced by one-pot redox cycles have been characterized quantitatively (Fig. 3 and figs. S7 to S16 and S23 to S29) using $^1$H NMR spectroscopy and $^1$H-$^1$H correlation spectroscopy (COSY) with mesitylene as an internal standard. Integration of the resulting $^1$H NMR spectra allowed us to calculate the $M_n$ values of the homologous series (Table 1) of these poly[*n*]rotaxanes. These calculated results are in good agreement with the theoretical $M_n$.

We also used 2D diffusion-ordered spectroscopy (DOSY) (figs. S30 to S35) and nuclear Overhauser effect spectroscopy (NOESY) measurements (figs. S36 to S40) to confirm the mechanically interlocked nature of the poly[*n*]rotaxanes. It is clear from Fig. 3, A to E, that the resonances for the $-OCH_2CH_2-$ repeating units in the PEG backbones undergo a continuous upfield shift with the increasing number of rings, as a result of the amplification of the shielding effect exerted by the $CBPQT^{4+}$ rings. The number of threaded rings can be estimated from the integration of probe resonances in the $^1$H NMR spectra recorded in Fig. 3. The ratio of the rings to the polymer dumbbell is deduced from carrying out comparisons between the expected integration values (numbers in parentheses in Fig. 3) and the actual values (numbers under peaks in Fig. 3) of proton resonances present in both the mechanically interlocked $CBPQT^{4+}$ rings ($H_{\alpha'}$, $H_{\beta'}$, $H_{Phen'}$, and $H_{CH2'}$) and the $PolyDB^{6+}$ components ($H_{6'}$, $H_{9'}$, $H_{7'}$, $H_{8'}$, and $H_{10'}$). In all five cases, the actual integrated values of the proton

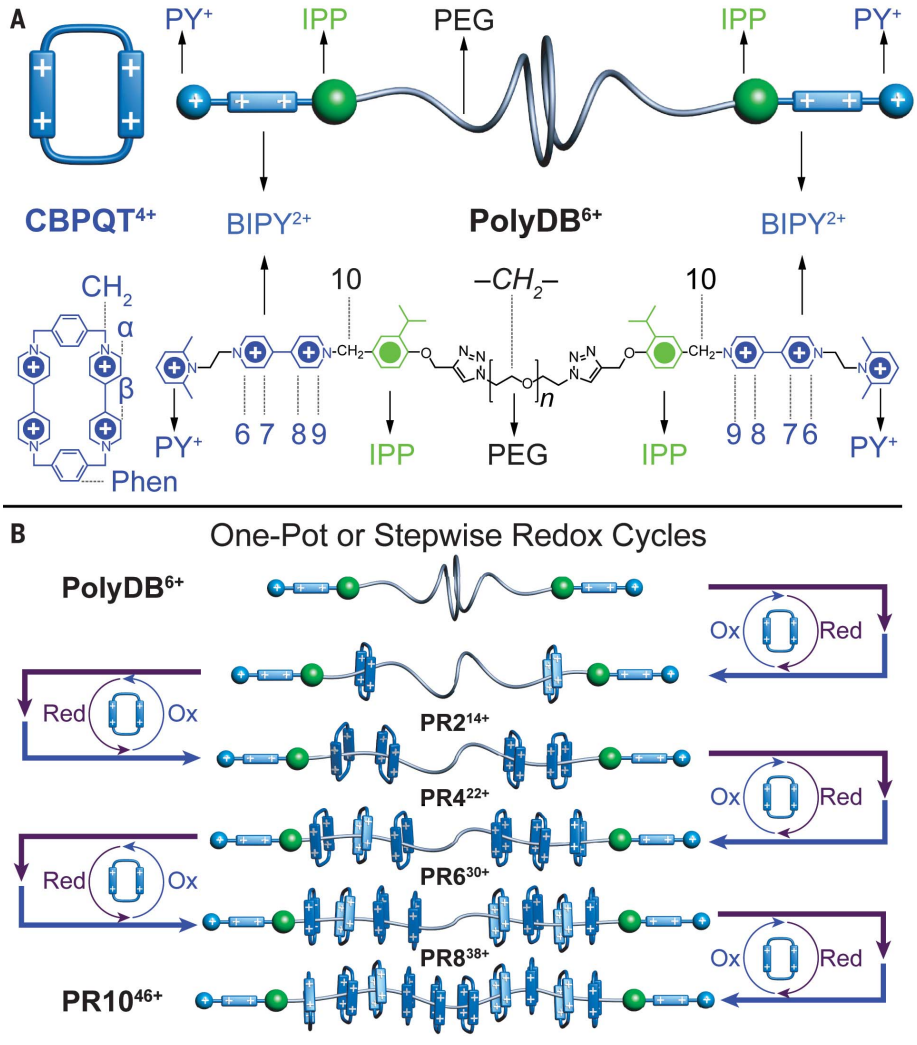


**Fig. 1. Graphical representations of the structural formulas for the CBPQT$^{4+}$ ring and PolyDB$^{6+}$, and the redox-driven syntheses of poly[*n*]rotaxanes using AMPs.** (**A**) Schematic representations of the structural formulas for the **CBPQT**$^{4+}$ ring and **PolyDB**$^{6+}$, which consists of two molecular pumps attached at both ends of the PEG chains through a pair of triazole rings, forming a collecting polymer chain located in the middle between the two pumps. The $PF_6^-$ counterions are omitted for the sake of clarity. Selected key protons on **CBPQT**$^{4+}$ (Phen, $CH_2$, α, and β) and **PolyDB**$^{6+}$ (numbers 6 to 10) are labeled to aid the interpretation of $^1$H NMR spectra reproduced in Fig. 3. The assignments of all proton resonances of **PolyDB**$^{6+}$ are labeled in fig. S3. (**B**) Schematic representation of the repetitive reduction and oxidation processes, either stepwise or in a one-pot synthesis, producing a series of polyrotaxanes **PR2**$^{14+}$, **PR4**$^{22+}$, **PR6**$^{30+}$, **PR8**$^{38+}$, and **PR10**$^{46+}$ with 2, 4, 6, 8, and 10 rings, respectively.

Corrected 11 June 2020. See full text.



resonances are in good agreement with the expected ones, thus indicating the successful threading of the rings onto PolyDB$^{6+}$ with the targeted number (2, 4, 6, 8, and 10). Among these $^1$H NMR spectra, those (Fig. 3, D and E) of **O-PR8**$^{38+}$ and **O-PR10**$^{46+}$ exhibit signal broadening attributable to the increased number of threaded rings, resulting in small deviations (figs. S11 and S14) between the expected and actual integrated values associated with the proton resonances for $H_{\beta'}$, $H_{7'}$, and $H_{8'}$. These deviations were mitigated after deconvolution to remove the integrations from irrelevant overlapping resonances (figs. S12 and S15), revealing excellent agreement between the actual integrated values and the expected ones.

To obtain unambiguous evidence of the co-constitutions of these poly[$n$]rotaxanes and determine the value of $n$ quantitatively, we used electrospray ionization-mass spectrometry (ESI-MS) of the polymer dumbbell precursor—the PEG bis(azide) ($M_n$ = 2000)—to probe the mass-to-charge ratio ($m/z$) distribution as a function of the different numbers of repeating $-OCH_2CH_2-$ units in each homogeneous collection of polymer chains. Three sets of signals, which are independently distributed without overlapping with each other, are observed (fig. S41) for the charge states ranging from 1+ to 3+, corresponding to $[M+Na]^+$, $[M+2Na]^{2+}$, and $[M+2H+Na]^{3+}$, respectively. This information lays the foundation for an in-depth analysis of **PolyDB**$^{6+}$ and the derived poly[$n$]rotaxanes. The ESI-MS analysis of **PolyDB**$^{6+}$ (Fig. 4A, purple) shows primarily four sets

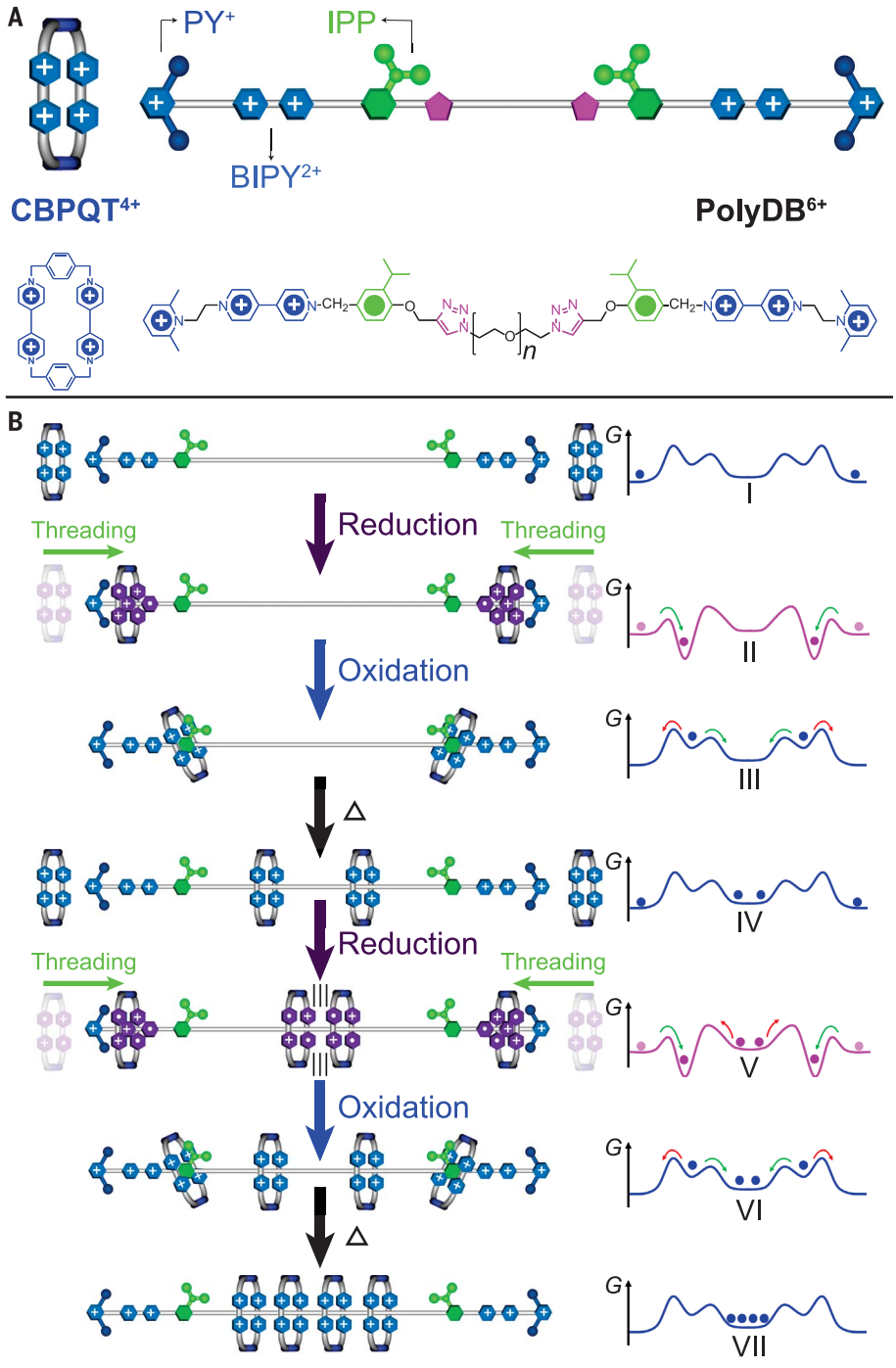


**Fig. 2. Graphical representations of the redox-driven synthesis of the poly[5]rotaxane by means of a flashing energy-ratchet mechanism.** (**A**) Graphical representations of the structural formulas for the **CBPQT**$^{4+}$ ring and **PolyDB**$^{6+}$, which consists of two molecular pumps attached at both ends of the PEG chains by a pair of triazole rings, forming a collecting polymer chain located in the middle between the two pumps. The $PF_6^-$ counterions are omitted for the sake of clarity. (**B**) The pumping mechanism for the redox-driven synthesis of the poly[5]rotaxane. Energy profiles representing the free energies of the system, as the rings are pumped in pairs onto the polymer dumbbell, are illustrated to the right of each intermediate in the reaction sequence. The curved arrows on the energy profiles represent reaction pathways that are either kinetically favored (green) or disfavored (red). The triazole rings (magenta) in each intermediate of the reaction are omitted for the sake of clarity. Initially (I), the rings and the polymer dumbbell repel each other because of strong coulombic repulsions. Upon reduction (II), all BIPY$^{2+}$ units are reduced to their radical cationic states (BIPY$^{+\bullet}$), leading to the threading of two **CBPQT**$^{2(+\bullet)}$ rings, one onto each end of **PolyDB**$^{4(+)2(\cdot)}$ with the formation of two trisradical tricationic complexes. Upon oxidation (III), the strong coulombic repulsions between the charged PY$^+$, BIPY$^{2+}$, and CBPQT$^{4+}$ units lead to the rings traversing the IPP steric barriers as a result of thermal energy, and falling into a kinetic trap provided by the collecting polymer chain, resulting in the formation (IV) of the poly[3]rotaxane. The second reduction (V) allows the pumps to recruit two more rings from the bulk solution by a similar mechanism. (In addition, the two threaded reduced rings most likely interact through radical-pairing interactions, indicated by a pair of triple vertical lines.) The second oxidation (VI) restores full charges to the BIPY$^{2+}$ units and the CBPQT$^{4+}$ rings and forces the second pair of rings to traverse the IPP steric barriers while the two reoxidized threaded rings are prevented from dethreading by these steric barriers, aided by the strong coulombic repulsions associated with both pumps. The second thermal relaxation results in the formation (VII) of the poly[5]rotaxane, and so on.

Corrected 11 June 2020. See full text.



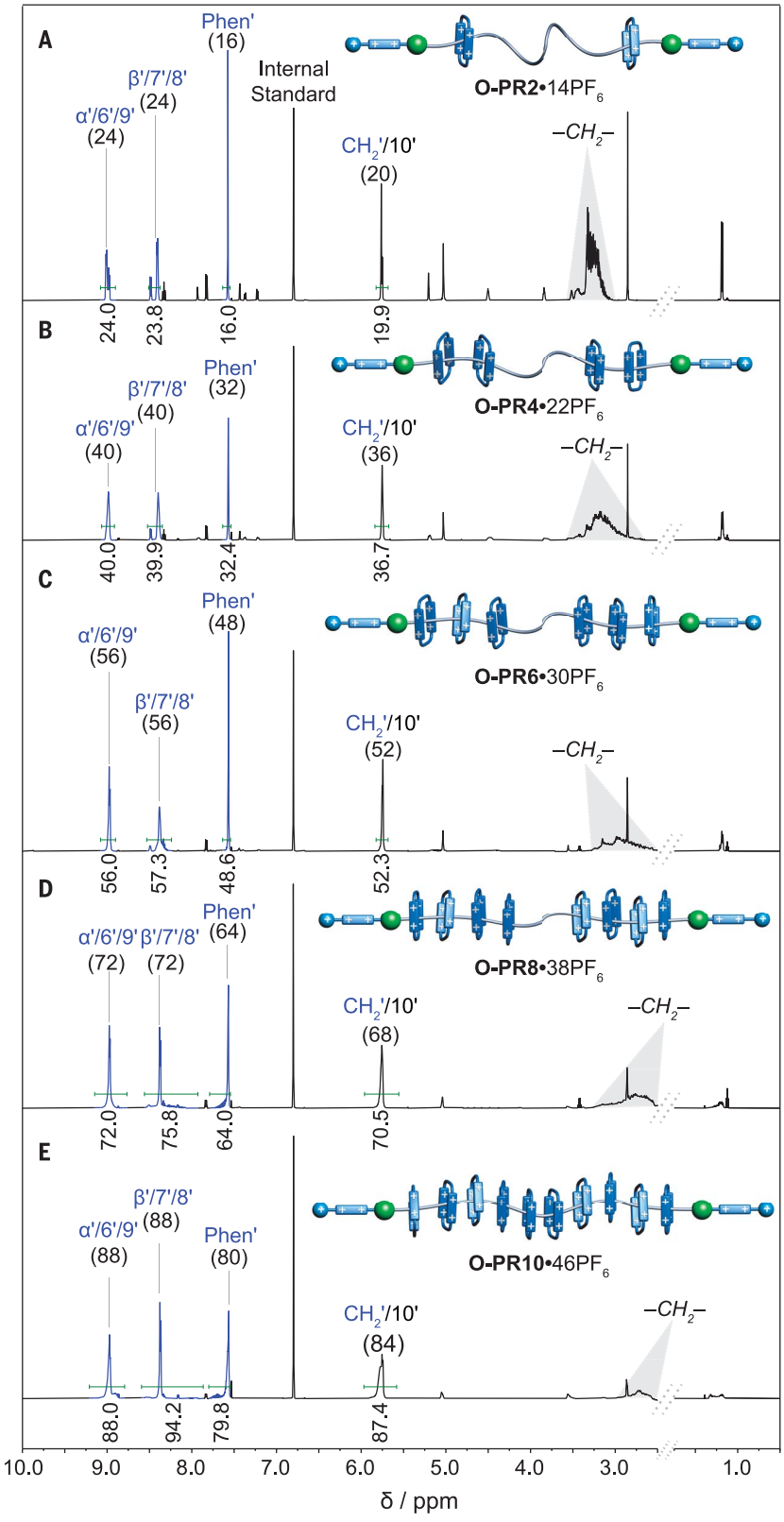


**Fig. 3. NMR spectroscopic characterization of all five poly[*n*]rotaxanes.** (**A**) Partial $^1$H NMR spectrum (600 MHz, $CD_3CN$, 298 K) of **O-PR2**$^{14+}$. (**B**) Partial $^1$H NMR spectrum (600 MHz, $CD_3CN$, 298 K) of **O-PR4**$^{22+}$. (**C**) Partial $^1$H NMR spectrum (600 MHz, $CD_3CN$, 298 K) of **O-PR6**$^{30+}$. (**D**) Partial $^1$H NMR spectrum (600 MHz, $CD_3CN$, 298 K) of **O-PR8**$^{38+}$. (**E**) Partial $^1$H NMR spectrum (600 MHz, $CD_3CN$, 298 K) of **O-PR10**$^{46+}$. Numbers in parentheses represent the expected integration values of the proton resonances of interest; numbers under the peaks represent the actual integrated values. Primes denote the proton resonances of mechanically interlocked molecules.

of signals ranging from 3+ to 6+, with each peak matching the chemical composition of $[(C_{66}H_{76}N_{12}O_2)(C_2H_4O)_n(PF_6^-)_x]^{(6-x)+}$ (fig. S42 and tables S1 to S4). Another set of signals with the charge state 4+ is also observed (Fig. 4A, green) as a result of the fragmentation of **PolyDB**$^{6+}$. We reasoned that under the mass spectrometric conditions, the BIPY$^{2+}$ units become labile and fragment from one or both ends, generating polymer dumbbells terminated by benzylic cations and the cleaved monobipyridinium fragments (fig. S43). To verify this hypothesis, we applied harsher ESI conditions by increasing both the sampling and extraction cone voltages. A singly charged peak with $m/z$ = 436.14 appears (fig. S44) as expected, with the isotope pattern matching the theoretical simulation of a dissociated monobipyridinium unit. The ESI-MS analysis of **O-PR2**$^{14+}$ shows the existence of three species (Fig. 4B, fig. S50, and tables S5 to 10). The 5+ and 6+ peaks (Fig. 4B, purple) correspond to the intact poly[3]rotaxane, whereas the green and blue signals are consequences of the fragmentations at one and both ends, respectively. The dissociation of the BIPY$^{2+}$ units from the polymer dumbbells does not jeopardize the mechanically interlocked nature of the poly[3]rotaxane because of the steric hindrance provided by the IPP units. Taken overall, these results, together with the $^1$H NMR spectroscopic analysis (Fig. 3A), indicate clearly that only two rings are pumped onto each individual polymer dumbbell after one redox cycle.

Analyses of **O-PR4**$^{22+}$, **O-PR6**$^{30+}$, and **O-PR8**$^{38+}$ (Fig. 4, C to E) also reveal mass spectra with primarily two sets of signals corresponding to the same fragmentations. Even though the peaks for intact poly[*n*]rotaxanes are hardly observable, possibly as a result of the diminished stability of the BIPY$^{2+}$ units in the case of the larger poly[*n*]rotaxanes, the mechanically interlocked characteristics of these poly[*n*]rotaxanes remain intact. Each charge state shows a clear mass distribution assignable to different numbers of repeating –$OCH_2CH_2$– units (figs. S51 to S56 and tables S11 to S24). The peaks observed in the spectra can only be assigned to **O-PR4**$^{22+}$, **O-PR6**$^{30+}$, and **O-PR8**$^{38+}$ with the corresponding four, six, and eight rings (*36*) mechanically interlocked with each individual polymer dumbbell, respectively.

**O-PR10**$^{46+}$, which has the largest molecular weight among the as-synthesized poly[*n*]rotaxanes, was also analyzed using ESI-MS, revealing a spectrum with only two series of charge states (Fig. 4F). Despite fragmentation, each peak, after deconvolution, matches the chemical composition of the fragmented **O-PR10**$^{46+}$, with the number of repeating –$OCH_2CH_2$– units representing the only difference (figs. S57 and S58 and tables S25 to S28). It is also evident from careful comparison (figs. S59 and S60) between

Corrected 11 June 2020. See full text.



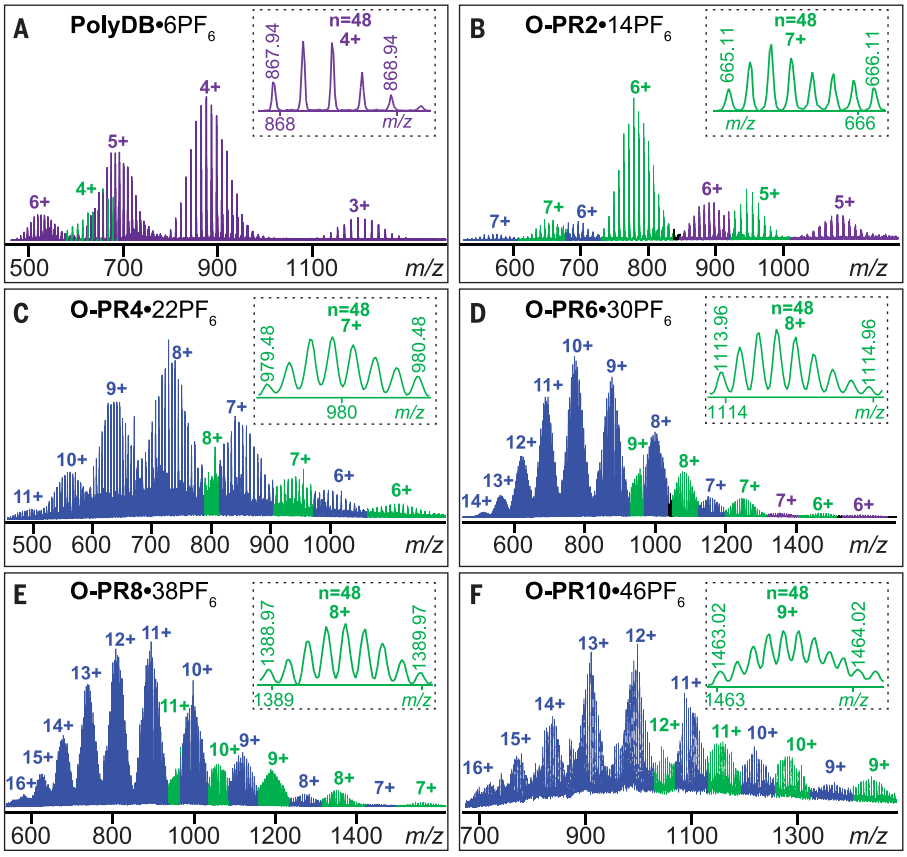


**Fig. 4. Electrospray ionization-mass spectrometry (ESI-MS) measurements of PolyDB•6PF$_6$ and all five poly[*n*]rotaxanes.** (**A**) ESI-MS for **PolyDB**•6PF$_6$. The inset shows the isotope pattern for [(**PolyDB**)•2PF$_6$]$^{4+}$ with 48 repeating –OCH$_2$CH$_2$– units. (**B** to **F**) ESI-MS full spectra for **O-PR2**•14PF$_6$ (B), **O-PR4**•22PF$_6$ (C), **O-PR6**•30PF$_6$ (D), **O-PR8**•38PF$_6$ (E), and **O-PR10**•46PF$_6$ (F). The insets show the isotope pattern for [(**O-PR2**)*•7PF$_6$]$^{7+}$, [(**O-PR4**)*•15PF$_6$]$^{7+}$, [(**O-PR6**)*•22PF$_6$]$^{8+}$, [(**O-PR8**)*•30PF$_6$]$^{8+}$, and [(**O-PR10**)*•37PF$_6$]$^{9+}$, respectively, with their corresponding charge states. The asterisk represents fragmentation at one end. The differences of these charge states in each spectrum result from the losses of different numbers of counterions (PF$_6^-$), and the distributions in charge states derive from PEG with different numbers of repeating units. Fragmentations at one or two ends are colored green and blue, respectively. The intact poly[*n*]rotaxanes without fragmentations are colored purple.

the two ESI-MS spectra (Fig. 4, E and F) that a trace amount of **O-PR8**$^{38+}$ is present in the sample of **O-PR10**$^{46+}$. This observation implies that the polyrotaxanes with shorter collecting chains could already have reached the steady state in which two threaded CBPQT$^{2(+\bullet)}$ rings on the collecting chain move to encircle the BIPY$^{+\bullet}$ units under reducing conditions and then move back to the collecting chain upon oxidation. Nonetheless, the findings from ESI-MS lend strong support to the successful one-pot precision synthesis of **O-PR10**$^{46+}$ with a well-defined number (10) of rings, affording out-of-equilibrium polycationic poly[11]rotaxane with high charge densities (46+) on single polymer chains.

With both stepwise and one-pot chemical redox synthetic strategies established, we turned our attention to developing an additional protocol that could potentially mitigate the accumulation of waste products resulting from the repetitive additions of redox reagents. Recently, we demonstrated (*37*) the use of electricity to operate AMPs in controlled potential electrolysis. Cyclic voltammograms (CVs) of all the poly[*n*]rotaxanes, which revealed nearly identical first reduction potentials, prove (fig. S68) that a similar standard electrochemical protocol using a reduction potential of –0.7 V during electrolysis should be applicable to the production of higher-order poly[*n*]rotaxanes. Ultimately, application of the electrochemical synthetic protocol in a stepwise and controlled manner leads to the production of the poly[*n*]rotaxanes **E-PR2**$^{14+}$, **E-PR4**$^{22+}$, **E-PR6**$^{30+}$, and **E-PR8**$^{38+}$ [(*38*); **E** denotes electrochemical] that are identical in comparison with the chemically synthesized poly[*n*]rotaxanes **O-PR2**$^{14+}$, **O-PR4**$^{22+}$, **O-PR6**$^{30+}$, and **O-PR8**$^{38+}$, respectively. All these electrochemically produced poly[*n*]rotaxanes were fully characterized by $^1$H NMR spectroscopy (figs. S17 to S21) and ESI-MS (figs. S61 to S67), including confirmation of the targeted number of rings, thereby highlighting the robustness and reliability of AMP-enabled precision synthesis of poly[*n*]rotaxanes by electrochemical means.

Finally, as the number of rings mechanically interlocked along the polymer dumbbells increases with the number of redox cycles, the random-coil backbones of PEG could become progressively more rigid and manifest an increase in their hydrodynamic diameters ($D_h$). Accordingly, we performed additional experiments, including DOSY, size exclusion chromatography (SEC), and dynamic light scattering (DLS) to probe the differences in size of **PolyDB**$^{6+}$ and the derived poly[*n*]rotaxanes. As anticipated, the 2D DOSY experiments (Table 1 and figs. S30 to S35) revealed a steady decrease in the diffusion constant, from 4.11 × $10^{-6}$ cm$^2$/s for **PolyDB**$^{6+}$ to 2.30 × $10^{-6}$ cm$^2$/s for **O-PR10**$^{46+}$, indicating an increase in $D_h$. The SEC elution profiles (figs. S75 to S81) show a decrease in elution time with increasing number of rings. The DLS data (Table 1 and figs. S69 to S74 and S81) confirm the increase in $D_h$, ranging from 2.67 ± 1.02 nm for **PolyDB**$^{6+}$ to 4.75 ± 1.38 nm for **O-PR10**$^{46+}$. We also carried out zeta potential measurements (Table 1), which show an increasing value from 0.77 ± 1.16 mV for **PolyDB**$^{6+}$ to 14.47 ± 0.35 mV for **O-PR10**$^{46+}$ as the charges accumulate rapidly with the increasing number of threaded rings. These observations, taken as a whole, confirm the progressive increase in hydrodynamic diameters from **PolyDB**$^{6+}$ to **O-PR10**$^{46+}$ as a direct result of the accumulation of the threaded rings with a number precisely defined.

The sequential installation of up to 10 rings onto the polymer dumbbell **PolyDB**$^{6+}$ is an example of redox-driven self-assembly (*39*) (Fig. 1B). From a thermodynamic perspective, the most probable structure arising from five cycles of pumping is **PR10**$^{46+}$, a highly unstable and energetic far-from-equilibrium polyrotaxane. Without pumping, the most probable structure is the polymer dumbbell **PolyDB**$^{6+}$ because of the decrease in entropy upon threading a pair of rings onto the collecting polymer chain. The redox-driven pumping process, by alternating reduction and oxidation consecutively, inputs energy into the system, which drives the resulting polyrotaxanes away from equilibrium. After oxidation, a pair of rings undergoes thermally activated relaxation, either back into the bulk solution over the PY$^+$ units (very unlikely) or onto the collecting chain over the IPP units (extremely likely) as a result of the large free energy for rings encircling the BIPY$^{2+}$ units after oxidation. A steady-state regime will be eventually reached after many cycles of redox reactions, where the likelihood of a ring escaping to the bulk solution from the

Corrected 11 June 2020. See full text.



**Table 1. Molar mass and physical constants of the polymer dumbbell and the derived poly[*n*] rotaxanes.** Theoretical and $^1$H NMR–derived number-average molecular weights ($M_n$), diffusion constants ($D$), hydrodynamic diameters ($D_h$), and zeta potentials (ζ) are shown for **PolyDB$^{6+}$**, **O-PR2$^{14+}$**, **O-PR4$^{22+}$**, **O-PR6$^{30+}$**, **O-PR8$^{38+}$**, and **O-PR10$^{46+}$**. Errors are reported as 1 SD. The theoretical $M_n$ of each sample where the counterions are $PF_6^-$ was estimated on the basis of the assumption that the molecular weight of the collecting polymer chain is 2000 g/mol. $^1$H NMR and DOSY spectra were measured in $CD_3CN$ on samples where the counterions were $PF_6^-$, whereas dynamic light scattering and zeta potential measurements were conducted in phosphate-buffered saline with either $TFA^-$ or $Cl^-$ as the counterions.

| Sample | PolyDB$^{6+}$ | O-PR2$^{14+}$ | O-PR4$^{22+}$ | O-PR6$^{30+}$ | O-PR8$^{38+}$ | O-PR10$^{46+}$ |
|---|---|---|---|---|---|---|
| Representation |  | | | | | |
| $M_n$ (theory) (g/mol) | 3800 | 6000 | 8200 | 10,400 | 12,600 | 14,800 |
| $M_n$ (NMR) (g/mol) | 4800 | 6200 | 9400 | 11,800 | 14,000 | 16,700 |
| $D$ (cm$^2$/s) | $4.11 \times 10^{-6}$ | $3.31 \times 10^{-6}$ | $2.86 \times 10^{-6}$ | $2.66 \times 10^{-6}$ | $2.48 \times 10^{-6}$ | $2.30 \times 10^{-6}$ |
| $D_h$ (nm) | 2.67 ± 1.02 | 2.74 ± 0.90 | 2.93 ± 1.09 | 4.02 ± 1.12 | 4.48 ± 0.74 | 4.75 ± 1.38 |
| ζ (mV) | 0.77 ± 1.16 | 3.14 ± 0.67 | 5.03 ± 0.58 | 6.50 ± 2.34 | 8.48 ± 0.44 | 14.47 ± 0.35 |

polymer dumbbell is equal to the likelihood of a ring being pumped from the bulk solution onto the polymer dumbbell—the process is a dynamic one—and the most likely outcome during a further redox cycle at steady state is that in which a pair of threaded $CBPQT^{2(+\bullet)}$ rings from the collecting chain moves to encircle the $BIPY^{+\bullet}$ units under reducing conditions and then simply moves back again onto the collecting chain upon oxidation. Although it is tempting to describe this process as "dissipative assembly," this description would be misleading. The key element that allows pumping to maintain a highly nonequilibrium structure is kinetic asymmetry (*40*) provided by the "pumping cassette" (*41*–*43*), which comprises a switchable barrier ($PY^+$), a switchable recognition site ($BIPY^{2+}/BIPY^{+\bullet}$), and a fixed neutral steric barrier (IPP). If the $PY^+$ units were substituted by the IPP units or vice versa, redox cycling would still dissipate energy but there would be no pumping of the rings onto the polymer dumbbell. The most probable compound in the presence of redox cycling, without kinetic asymmetry, would be **PolyDB$^{6+}$** with no threaded rings. (See the supplementary materials for a more detailed discussion.)

The six positive charges of **PolyDB$^{6+}$**, already associated with the operational components of the pumps on the polymer dumbbells, can be augmented by another 8+ to 16+ to 24+ to 32+ to 40+ with the pairwise addition of two, four, six, eight, and 10 rings, respectively. Hence, emergent behavior on the part of the polyrotaxanes becomes a real possibility. This foray into ever-increasing nonequilibrium states raises unlimited questions and opens doors to a whole range of new directions that can be pursued in unnatural polymer synthesis. There is the opportunity to tune the materials properties of slide-ring polymers with more or fewer rings located at will, and almost free of noncovalent bonding interactions with the polymer dumbbells. The fact that palindromic arrays of co-constitutionally heterotopic rings can be positioned on constitutionally symmetrical dumbbells means that it is now possible to use polyrotaxanes, engineered in an appropriate manner, to transcribe their programmed information back into the domain of controlling, by the use of further templation, sequences of building blocks in a new line of wholly synthetic polymers. These possibilities represent little more than the tip of the iceberg.

## REFERENCES AND NOTES


1. J. F. Stoddart, *Angew. Chem. Int. Ed.* **56**, 11094–11125 (2017).
2. C. Pezzato, C. Cheng, J. F. Stoddart, R. D. Astumian, *Chem. Soc. Rev.* **46**, 5491–5507 (2017).
3. S. Erbas-Cakmak, D. A. Leigh, C. T. McTernan, A. L. Nussbaumer, *Chem. Rev.* **115**, 10081–10206 (2015).
4. C. J. Bruns, J. F. Stoddart, *The Nature of the Mechanical Bond: From Molecules to Machines* (Wiley, 2016).
5. S. Mena-Hernando, E. M. Pérez, *Chem. Soc. Rev.* **48**, 5016–5032 (2019).
6. A. Harada, A. Hashidzume, H. Yamaguchi, Y. Takashima, *Chem. Rev.* **109**, 5974–6023 (2009).
7. M. Arunachalam, H. W. Gibson, *Prog. Polym. Sci.* **39**, 1043–1073 (2014).
8. Z. Niu, H. W. Gibson, *Chem. Rev.* **109**, 6024–6046 (2009).
9. Q. Wu *et al*., *Science* **358**, 1434–1439 (2017).
10. Y. Noda, Y. Hayashi, K. Ito, *J. Appl. Polym. Sci.* **131**, 40509 (2014).
11. S. Choi, T.-w. Kwon, A. Coskun, J. W. Choi, *Science* **357**, 279–283 (2017).
12. K. K. Cotí *et al*., *Nanoscale* **1**, 16–39 (2009).
13. J. J. Li, F. Zhao, J. Li, *Appl. Microbiol. Biotechnol.* **90** 427–443 (2011).
14. F. M. Raymo, J. F. Stoddart, *Chem. Rev.* **99**, 1643–1664 (1999).
15. D. J. Cram, *Science* **240**, 760–767 (1988).
16. J.-M. Lehn, *Science* **295**, 2400–2403 (2002).
17. A. Harada, J. Li, M. Kamachi, *Nature* **356**, 325–327 (1992).
18. A. B. C. Deutman *et al*., *Science* **322**, 1668–1671 (2008).
19. F. M. Raymo, J. F. Stoddart, *Trends Polym. Sci.* **4**, 208–211 (1996).
20. P. R. Ashton, M. Bělohradský, D. Philp, J. F. Stoddart, *J. Chem. Soc. Chem. Commun.* **1993**, 1269–1274 (1993).
21. J. Wu, K. C.-F. Leung, J. F. Stoddart, *Proc. Natl. Acad. Sci. U.S.A.* **104**, 17266–17271 (2007).
22. M. E. Belowich *et al*., *J. Am. Chem. Soc.* **134**, 5243–5261 (2012).
23. N. Momčilović, P. G. Clark, A. J. Boydston, R. H. Grubbs, *J. Am. Chem. Soc.* **133**, 19087–19089 (2011).
24. S. Kang, M. M. Cetin, R. Jiang, E. S. Clevenger, M. F. Mayer, *J. Am. Chem. Soc.* **136**, 12588–12591 (2014).
25. M. D. Cornelissen *et al*., *J. Org. Chem.* **85**, 3146–3159 (2020).
26. J. E. M. Lewis, J. Winn, L. Cera, S. M. Goldup, *J. Am. Chem. Soc.* **138**, 16329–16336 (2016).
27. K. Mayumi, K. Ito, K. Kato, *Polyrotaxane and Slide-Ring Materials* (RSC, 2016).
28. C. Cheng *et al*., *Nat. Nanotechnol.* **10**, 547–553 (2015).
29. C. Pezzato *et al*., *Tetrahedron* **73**, 4849–4857 (2017).
30. Y. Qiu *et al*., *J. Am. Chem. Soc.* **141**, 17472–17476 (2019).
31. R. D. Astumian, I. Derényi, *Eur. Biophys. J.* **27**, 474–489 (1998).
32. Considering the MW ($M_n$ = 2000) of the PEG, which has around 45 $-OCH_2CH_2-$ repeating units, we estimate that no more than 17 rings can be pumped, ignoring electrostatic interactions, onto the collecting polymer chains (*28*, *29*), as each ring occupies approximately a length on the chain that equates to ~8 atoms.
33. H. C. Kolb, M. G. Finn, K. B. Sharpless, *Angew. Chem. Int. Ed.* **40**, 2004–2021 (2001).
34. Y. Wang, M. Frasconi, J. F. Stoddart, *ACS Cent. Sci.* **3**, 927–935 (2017).
35. As demonstrated previously (*28*, *29*), a reduction time of 10 min with Zn dust is more than sufficient to complete the reduction/threading and power the molecular pump. In actual fact, we set the time for the reduction in the present investigation at 30 min in order to achieve exhaustive complexation of a pair of rings onto the pumps. Additionally, taking into consideration the fact that cobaltocene is a stronger reducing reagent than Zn, allowing 30 min for the reduction is more than enough to complete the reduction of all the $BIPY^{2+}$ units.
36. It has been noted that a trace amount of polyrotaxanes with an odd number of rings is present in the ESI-MS spectra of **S-PR6$^{30+}$** (fig. S48), **O-PR4$^{22+}$** (fig. S51), **O-PR8$^{38+}$** (fig. S55), and **E-PR6$^{30+}$** (fig. S64).
37. C. Pezzato *et al*., *Angew. Chem. Int. Ed.* **57**, 9325–9329 (2018).
38. ESI-MS failed to provide convincing evidence of the exact number of rings on the electrochemically synthesized **E-PR10$^{46+}$**. However, the $^1$H NMR spectrum of **E-PR10$^{46+}$** (fig. S21) reveals a structure similar to that of **O-PR10$^{46+}$** (fig. S13), which is obviously different from that of its starting material **E-PR8$^{38+}$** (fig. S20).
39. G. Ragazzon, L. J. Prins, *Nat. Nanotechnol.* **13**, 882–889 (2018).
40. R. D. Astumian, *Nat. Commun.* **10**, 3837 (2019).
41. R. D. Astumian, B. Robertson, *J. Am. Chem. Soc.* **115**, 11063–11068 (1993).
42. S. Erbas-Cakmak *et al*., *Science* **358**, 340–343 (2017).
43. G. Ragazzon *et al*., *Nat. Nanotechnol.* **10**, 70–75 (2015).


## ACKNOWLEDGMENTS

We thank Y. Zhang for help with NMR measurements, A. Gaisin for help with SEC measurements, and T. Kosikova, H. Sun, X. Zhou, and W. Cao for discussions. **Funding:** We thank Northwestern University for its continued support of this research. B.S. and X.L. were supported by NIH grant R01GM128037. This work made use of the Integrated Molecular Structure Education and Research Center (IMSERC) at Northwestern University, which has received support from the Soft and Hybrid Nanotechnology Experimental (SHyNE) Resource (NSF ECCS-1542205), the State of Illinois, and the International Institute for Nanotechnology (IIN). The Bruker 600 MHz NMR spectrometer used in this work is partially funded by NIH grant 1S10OD012016-01. This work made use of the Keck-II facility of Northwestern University's NU*ANCE* Center, which has received support from the SHyNE Resource (NSF ECCS-1542205),

the MRSEC program (NSF DMR-1720139) at the Materials Research Center, IIN, the Keck Foundation, and the State of Illinois through IIN. Use of resources of the Keck Biophysics Facility was supported in part by National Cancer Institute award CCSG-P30-CA060553 to the Robert H. Lurie Comprehensive Cancer Center at Northwestern University. **Author contributions:** Y.Q., C.P., C.C., and J.F.S. conceived the study; Y.Q. and J.F.S. designed experiments; Y.Q. conducted the synthesis, NMR, CV, DLS, SEC, and zeta potential analysis; B.S. and X.L. conducted ESI-MS measurements and analysis; D.S. contributed to the graphical design in figures; W. Liu conducted ITC measurements, NMR titration experiments, and NMR analysis; C.P. and Y.F. provided part of the synthetic precursors; C.P., D.S., W. Liu, L.Z., Y.F., Q.-H.G., K.C., W. Li, H.C., M.T.N., Y.S., and R.D.A. commented on the data and all authors contributed to data analysis; and Y.Q. and J.F.S. wrote the draft with input from all authors. **Competing interests:** Y.Q. and J.F.S. have a patent application lodged with Northwestern University (INVO Reference No. NU 2020-106) based on this work. **Data and materials availability:** All data are available in the main text or the supplementary materials.

## SUPPLEMENTARY MATERIALS



20 February 2020; resubmitted 5 April 2020
Accepted 27 April 2020
10.1126/science.abb3962

Science

# A precise polyrotaxane synthesizer

Yunyan QiuBo SongCristian PezzatoDengke ShenWenqi LiuLong ZhangYuanning FengQing-Hui GuoKang CaiWeixingyue LiHongliang ChenMinh T. NguyenYi ShiChuyang ChengR. Dean AstumianXiaopeng LiJ. Fraser Stoddart

*Science*, 368 (6496), • DOI: 10.1126/science.abb3962

**Ten rings on one axle**

Rotaxanes consist of molecular rings threaded on a central axle. Most approaches to their synthesis have focused on introducing a single ring per axle. Qiu *et al.* now report a systematic approach to threading up to 10 adjacent rings consecutively. The axle's end groups were constructed to attract free-floating rings when reduced and then to push those rings toward the center upon oxidation. Products of each successive reduction-oxidation cycle were characterized by nuclear magnetic resonance spectroscopy and mass spectrometry.

*Science*, this issue p. 1247



*Science* (ISSN 1095-9203) is published by the American Association for the Advancement of Science. 1200 New York Avenue NW, Washington, DC 20005. The title *Science* is a registered trademark of AAAS.